ACS Energy LETTERS

http://pubs.acs.org/journal/aelccp

A Self-Trapping, Bipolar Viologen Bromide Electrolyte for Redox Flow Batteries

Wenda Wu, Jian Luo, Fang Wang, Bing Yuan, and T. Leo Liu*

Cite This: *ACS Energy Lett.* 2021, 6, 2891–2897

Read Online

ACCESS | Metrics & More | Article Recommendations | Supporting Information

ABSTRACT: Aqueous organic redox flow batteries (AORFBs) have become increasingly attractive for scalable energy storage. However, it remains challenging to develop high-voltage, powerful AORFBs because of the lack of a high redox potential catholyte. Herein, we report methyl viologen dibromide ($[MV]Br_2$) as a facile self-trapping, bipolar redox electrolyte material for pH-neutral redox flow battery applications, representing the first report of methyl viologen as a highly efficient bromine complexing reagent. The formation of the $[MV](Br_3)_2$ complex was computationally predicted and experimentally confirmed. The low-solubility $[MV](Br_3)_2$ complex in the catholyte during the battery charge process not only mitigates the crossover of charged tribromide species (Br_3^-) but also addresses the toxicity concern of volatile bromine simultaneously. A 1.53 V bipolar MV/Br AORFB (10.2 Wh/L) delivered stable battery performance at pH-neutral conditions, specifically, 100% total capacity retention, 133 mW/cm^2 power density, and 56% energy efficiency at 60 mA/cm^2.

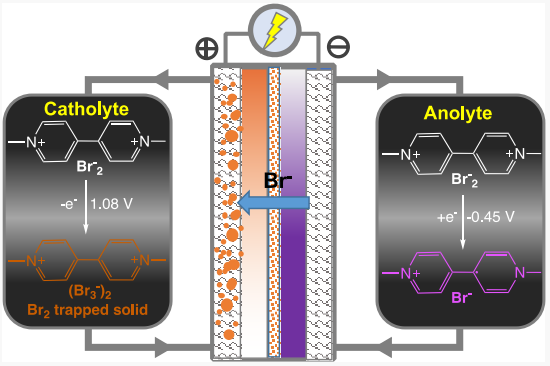

In the last decades, the development of environmentally friendly renewable energy resources has grown rapidly to achieve a sustainable society. To efficiently utilize intermittent energies such as solar and wind, advanced energy storage technologies are in high demand.[1−4] Redox flow batteries (RFBs, Scheme 1A) are favorably attractive for scalable and dispatchable energy storage because of their advantages of decoupled energy and power, high current and power performance, and nonflammable and low-cost aqueous supporting electrolytes.[1−5] Traditional aqueous inorganic RFBs (AIRFBs) employing inorganic redox-active compounds including metal salts and halides as energy storage materials have received massive attention.[2] However, materials challenges of AIRFBs, including expensive active materials, corrosive electrolytes, limited tunability, and parasitic reactions such as hydrogen evolution prevent their widespread implementation and acceptance by industries.[1,3,4] To achieve economic and environmentally benign energy storage, tunable and sustainable redox-active organic electrolyte materials[6−18] have been developed for aqueous RFB applications in recent years.[1,3,4]

Scheme 1. (A) Schematic Illustration of the Bipolar MV/Br AORFB and (B) Molecular Structure of $[MV]Br_2$ and Its Technical Merits for Flow Battery Applications

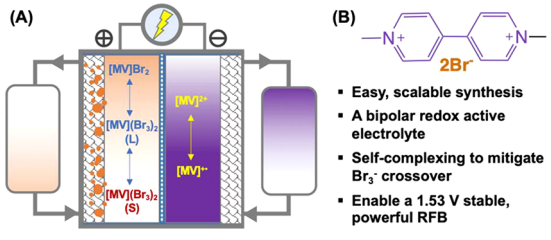

We and other groups have demonstrated that viologen molecules, because of outstanding stability and high charge capacities, are privileged anolyte materials for pH-neutral aqueous organic redox flow batteries.[1] Viologen compounds have been paired with TEMPO,[8,19] ferrocene,[10,20−22] ferrocyanide,[12] and iodide[23] for pH-neutral AORFBs which delivered reliable current performance and superior cycling stability. Nevertheless, owing to the low redox potential of iodide ($E_{1/2}(I_3^-/I^-)$ = 0.57 V vs NHE), ferrocene derivatives such as (ferrocenylmethyl)trimethylammonium chloride ($E_{1/2}$ = 0.61 V, vs NHE), and ferrocyanide ($E_{1/2}([Fe(CN)_6]^{3-/4-})$ = 0.39 V vs NHE), these corresponding AORFBs could deliver only battery voltages of less than 1.06 V. It is desired to

Received: June 3, 2021
Accepted: June 30, 2021
Published: July 26, 2021

https://doi.org/10.1021/acsenergylett.1c01146
ACS Energy Lett. 2021, 6, 2891–2897

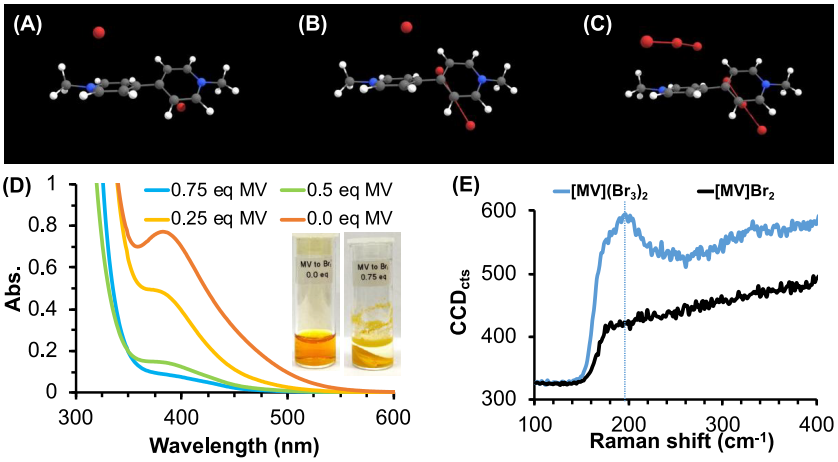

Figure 1. Computational and UV−vis studies of the bromine complexation of $[MV]Br_2$. Optimized structures of (A) $[MV]Br_2$, (B) $[MV](Br_3)Br$, and (C) $[MV](Br_3)_2$ and (D) UV−vis spectra for the $NaBr_3$ titration experiment with $[MV]Br_2$. All titrated samples were diluted five times before UV−vis tests. The fresh $NaBr_3$ sample (0.0 equiv of $[MV]Br_2$) was diluted 40 times from 0.25 M for measurement. Inserted photos illustrate the samples before and after the titration of 0.75 equiv of $[MV]Br_2$ to show the color change and the formation of precipitate. (E) Raman spectra of $[MV]Br_2$ and $[MV](Br_3)_2$ solid samples.

develop high-voltage AORFBs to boost energy and power densities simultaneously. Although viologen compounds have been paired with TEMPO compounds to achieve higher battery voltages, the insufficient stability and expensive synthesis cost of TEMPO derivatives limited their practical development.[24] Compared to iodide salts, bromide salts are more attractive halide catholyte materials as bromide has a more positive potential (1.08 V vs NHE) than iodide (0.57 vs NHE), and bromine has a higher earth-crust abundance (2.4 ppm) and a lower cost ($2.19/kg) than iodine (0.45 ppm for abundance and $26/kg for cost).[25,26] More recently, bromide salts have been exploited as high redox potential, high-capacity catholytes for viologen-based AORFBs.[24,27] We reported a high-voltage AORFB by pairing a sulfonate functionalized viologen compound, 1,1′-di(3-sulfonatopropyl)-4,4′-bipyridinium, $(SPr)_2V$, with a low-cost bromide catholyte (NH_4Br).[24] In the $(SPr)_2V$/Br AORFB, however, the cycling stability was hindered by the volatilization and crossover of the tribromide species (Br_3^-).[24]

To address the crossover and volatilization issues of bromine species, quaternary ammonium bromides were applied as complex reagents to trap the Br_3^- by complexation (typically forming a new liquid or solid phase) in battery studies.[28,29] Viologen molecules are dipyridinium salts and are analogous to quaternary ammonium salts. Thus, we hypothesized that viologen molecules could stabilize the Br_3^- anion and might be capable of working as a redox-active "self-trapping" reagent for viologen/Br AORFBs (eqs 1−3). On the anolyte side, viologen is charged to its radical state for electron storage. On the catholyte side, the Br_3^- species generated in the charge process is expected to be trapped by the viologen cation to form a viologen−bromine complex, e.g. $[MV](Br_3)_2$ in the case of methyl viologen cations (MV^{2+}). In addition, the bipolar nature of $[MV]Br_2$ (Scheme 1B) will allow the use of a low-cost porous separator instead of using an expensive ion exchange membrane as reported in the previous studies. Our results revealed that $[MV]Br_2$ can complex with Br_2 to form poorly soluble $[MV](Br_3)_2$ to mitigate the crossover of the tribromide species (Br_3^-) during flow battery operation. A 1.53 V bipolar MV/Br AORFB (10.2 Wh/L, Scheme 1A) demonstrated stable battery performance, including high stability (100% capacity retention for 100 cycles) and high power density (up to 133 mW/cm^2).

Anode:

$$[MV]^{2+} + e^- \rightleftarrows [MV]^{+} \quad (1)$$

Cathode:

$$0.25[MV]^{2+} + 1.5Br^- - e^- \rightleftarrows 0.25[MV(Br_3)_2]\downarrow \quad (2)$$

Full cell:

$$1.25[MV]^{2+} + 1.5Br^- \rightleftarrows [MV]^{+} + 0.25[MV(Br_3)_2]\downarrow \quad (3)$$

$$[MVBr_2] + Br_2 \rightleftarrows [MV(Br^-)(Br_3^-)] \quad \Delta G = -24.36 \text{ kcal/mol} \quad (4)$$

$$[MVBr_2] + 2Br_2 \rightleftarrows [MV](Br_3)_2 \quad \Delta G = -48.99 \text{ kcal/mol} \quad (5)$$

First, we proposed two reactions that the $[MV]^{2+}$ cation would complex with Br_3^- anions (eqs 4 and 5). Then, density functional theory (DFT) calculations at the M06-2x/6-31+G** level with the SMD solvation model were conducted to determine the most possible pattern by calculating thermal free energies of reactants and products. Figure 1A−C displays the optimized structures of $[MV]Br_2$ and its Br_2-complexing products, $[MV]Br_3Br$ and $[MV](Br_3)_2$. Br_3^- (or Br^-) anions are placed at each side of the bis-pyridinium moiety. Consistent with the ionic bonding interaction, Br^- anions are positioned about 3.30 Å from the N atoms of the $[MV]^{2+}$ cation in $[MV]Br_2$. After the complexing of Br_2, the distance between Br_3^- and N slightly increases to about 3.36 Å in $[MV]Br_3Br$ and $[MV](Br_3)_2$. According to DFT results, one $[MV]Br_2$ molecule can bind two Br_3^- anions with downhill free energy of −48.99 kcal/mol, which is two times more favorable than binding with one Br_3^- (eqs 4 and 5; see the Supporting Information for more computational details).

After confirming the hypothesis computationally, the bipolar $[MV]Br_2$ compound was prepared using 4,4′-bipyridine and bromoacetic acid in a yield of 95% at a scale of more than 20 g. $[MV]Br_2$ has a solubility of 2.1 M in water, which is much

https://doi.org/10.1021/acsenergylett.1c01146
ACS Energy Lett. 2021, 6, 2891−2897

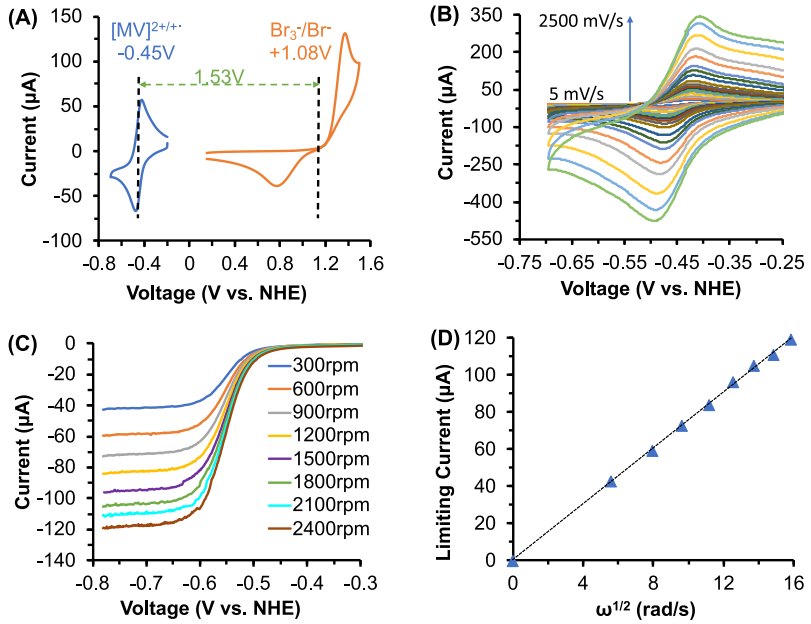

Figure 2. Electrochemical studies of $[MV]Br_2$. (A) Cyclic voltammograms of $[MV]Br_2$ with $[MV]^{2+}/[MV]^{+\cdot}$ at −0.45 V and Br^-/Br_3^- at 1.08 V. (B) Cyclic voltammograms of MV (scan rates from 5 to 2500 mV/s). Experimental conditions for panels A and B: 4.0 mM $[MV]Br_2$ in 0.5 M NaBr aqueous electrolyte, 100 mV/s scan rate, glassy carbon working electrode, carbon counter electrode, and Ag/AgCl reference electrode. (C) LSV scans using a glassy carbon rotating working electrode for the reduction of $[MV]Br_2$. Experimental conditions: 1.0 mM $[MV]Br_2$ in 0.5 M NaBr. (D) Levich plot based on the LSV data.

higher than that of $[MV]I_2$ (0.23 M). Then, the complexing efficiency of the $[\mathbf{MV}]^{2+}$ dication with Br_3^- was studied by UV−vis through a titration experiment. As is depicted in the photos in Figure 1D, a series of 0.25 M $NaBr_3$ solutions were titrated by $[\mathbf{MV}]\mathbf{Br_2}$ with an increasing concentration gradient, and the free Br_3^- concentration was determined by a calibration curve. As shown in Figure 1D, after 0.25 equiv of $[\mathbf{MV}]\mathbf{Br_2}$ was added, the free Br_3^- concentration decreased dramatically from 0.25 to 0.019 M, and it further decreased to 0.0047 M if 0.5 equiv of $[\mathbf{MV}]^{2+}$ was added. With 0.75 equiv of $[\mathbf{MV}]^{2+}$, the Br_3^- diagnostic absorbance peak at 386 nm became too weak to be observed, achieving a quantitative complexing efficiency. In the meanwhile, the formation of the solid-phase $[\mathbf{MV}](\mathbf{Br_3})_2$ was clearly observed. $[\mathbf{MV}](\mathbf{Br_3})_2$ exhibits a diagnostic Br_3^- stretch at 197.8 cm^{-1} in its Raman spectrum (Figure 1E). The bromine trapping by $[\mathbf{MV}]^{2+}$ was further confirmed using a reduction titration of $[\mathbf{MV}](\mathbf{Br_3})_2$ using $K_4[Fe(CN)_6]$ by UV−vis studies (Figures S1 and S2). The solubility of $[\mathbf{MV}](\mathbf{Br_3})_2$ was then measured by ^1H NMR as low as 20 mM in deionized water, as shown in Figure S3. It is noted that $[\mathbf{MV}](\mathbf{Br_3})_2$ displayed an ^1H NMR spectrum nearly identical to that of $[MV]Br_2$ (Figure S9A). The high sedimentation efficiency of $[\mathbf{MV}]^{2+}$ with Br_3^- and the low solubility of $[\mathbf{MV}](\mathbf{Br_3})_2$ precipitate credibly suggest a low possibility of Br_3^- crossover in the battery cycling process of a bipolar MV/Br AORFB, which would be a great enhancement for the battery's long-term stability. It should be noted that the formation of solid $[\mathbf{MV}](\mathbf{Br_3})_2$ phase is also beneficial to mitigate the toxic concerns surrounding volatile Br_2.

Next, we proceeded to study the electrochemical properties of the bipolar compound $[\mathbf{MV}]\mathbf{Br_2}$. Electrochemical properties of $[\mathbf{MV}]\mathbf{Br_2}$ in a NaBr supporting electrolyte were studied by cyclic voltammetry (CV) and linear sweep voltammetry (LSV) with rotating disc electrode (RDE). As shown in Figure 2A, both $[\mathbf{MV}]^{2+}$ cation and bromide anion exhibited reversible CV signals in aqueous solution with $E_{1/2}(MV) = -0.45$ V and $E_{1/2}(Br) = 1.08$ V (vs NHE), giving a 1.53 V battery voltage for the MV/Br AORFB. Scan dependence CV studies revealed that the separation of the cathodic and anodic waves of $[\mathbf{MV}]^{2+}$ remained a constant ca. 57 mV (Figure 2B), indicative of a fast electron-transfer rate. Then the electron-transfer rate constant (k^0) of $[\mathbf{MV}]^{2+}$ in the NaBr supporting electrolyte was estimated as 0.35 cm/s by Nicholson's method (see the Supporting Information for details). The diffusion coefficient (D) of $[\mathbf{MV}]^{2+}$ was calculated as 5.02×10^{-6} cm^2/s by the Levich equation using the RDE data (Figure 2C,D).

Then a bipolar $[\mathbf{MV}]\mathbf{Br_2}$ AORFB was first evaluated at 0.1 M for its energy storage performance at neutral pH conditions. Because of the bipolar nature of the $[\mathbf{MV}]\mathbf{Br_2}$ electrolyte, we used a commercial porous Daramic membrane as separator. It is worth noting that Daramic membrane (175 μm thickness) is inexpensive and has a much lower area resistance of 1.65 $\Omega \cdot cm^2$ (Figure S11) in comparison to the thinner benchmark AMV membrane (2.8 $\Omega \cdot cm^2$, 110 μm). The same electrolyte of 0.1 M $[\mathbf{MV}]\mathbf{Br_2}$ in 2.0 M NaCl with high conductivity of 174.5 mS/cm was used as the catholyte and anolyte. The $[\mathbf{MV}]\mathbf{Br_2}$ AORFB using the Daramic membrane was galvanostatically charged and discharged between 0.2 and 1.8 V from 20 to 100 mA/cm^2 (Figure 3A) and then followed with extended 100 charge−discharge cycles (Figure 3D, red curves). At 40 mA/cm^2, the $[\mathbf{MV}]\mathbf{Br_2}$ RFB was able to deliver an energy efficiency of 65% and a capacity utilization of 80%. It was observed that the charged catholyte $[\mathbf{MV}](\mathbf{Br_3})_2$ was primarily deposited on the surface of the graphite carbon electrode (see Figure S4). It is believed both solid and solution (20 mM) phases of $[\mathbf{MV}](\mathbf{Br_3})_2$ could proceed with the discharge step. Alternatively, the solid phase can go back to the solution phase and then undergo discharge (Scheme 1A). Interestingly, the solid-phase formation does not affect the current performance of the battery as it was cycled up to 100

https://doi.org/10.1021/acsenergylett.1c01146
ACS Energy Lett. 2021, 6, 2891−2897

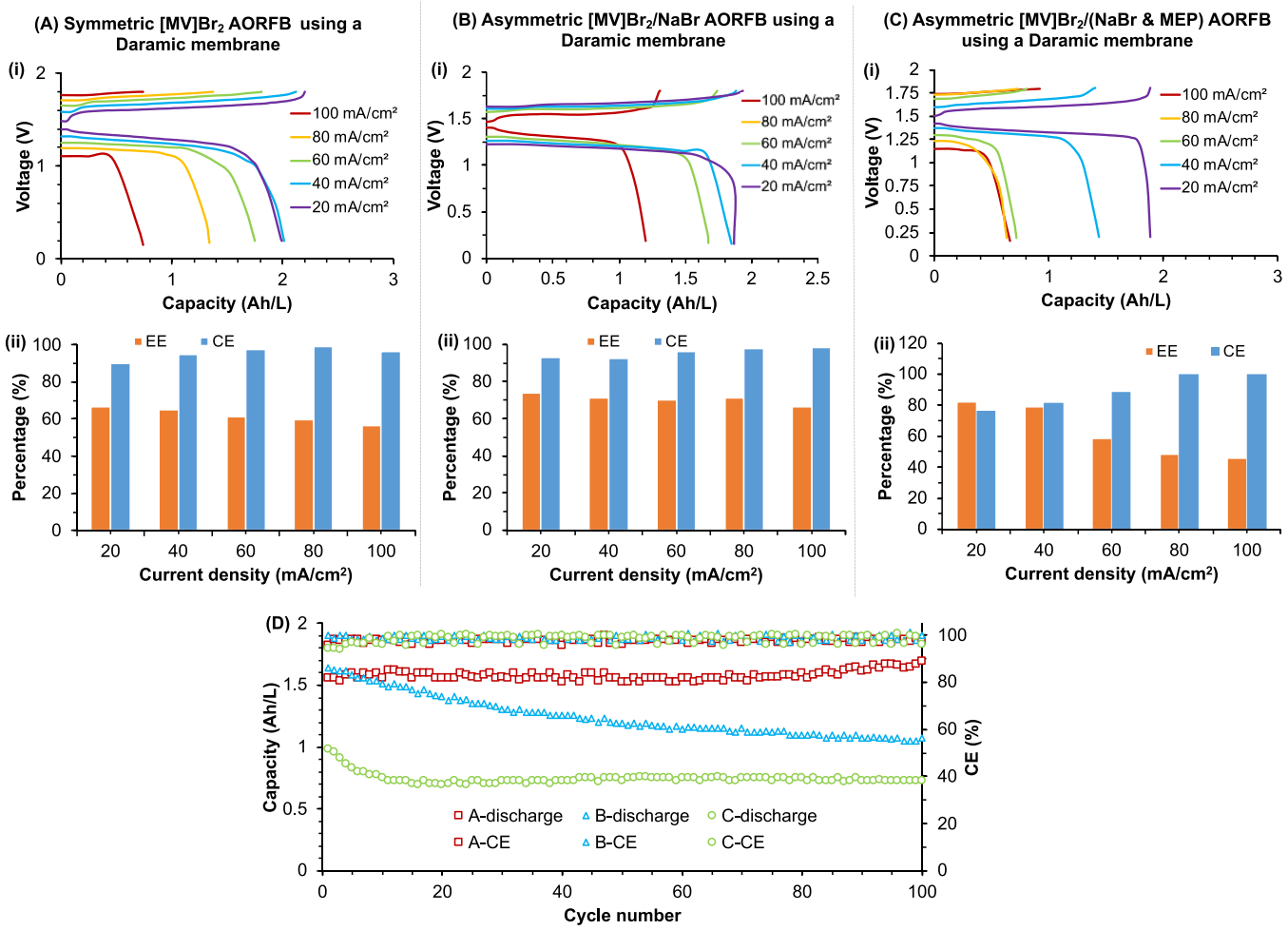

Figure 3. Cycling performance of the $[MV]Br_2$ electrolyte using different flow battery configurations. (A) 0.1 M symmetric $[MV]Br_2$ AORFB: 12 mL of 0.1 M $[MV]Br_2$ in 2.0 M NaCl as an anolyte/catholyte, and a Daramic membrane as separator. (B) 0.1 M asymmetric $[MV]Br_2$/NaBr AORFB: 12 mL 0.1 M $[MV]Br_2$ in 2.0 M NaCl as an anolyte, 12 mL of 0.2 M NaBr in 2.0 M NaCl as a catholyte, and a Daramic membrane as separator. (C) 0.1 M asymmetric $[MV]Br_2$ AORFB: 12 mL of 0.1 M $[MV]Br_2$ in 2.0 M NaCl as an anolyte, 12 mL of 0.2 M NaBr with 0.1 M MEP in 1.8 M NaCl as a catholyte, and a Daramic membrane as separator. (i) Charge−discharge curves and (ii) energy efficiency (EE) and Columbic efficiency (CE) at different current densities for the flow batteries described in panels A−C. (D) Extended cycling tests for 100 cycles after the rate performance tests of the three flow batteries.

mA/cm^2 with an energy efficiency of 56.25%. In the extended cycle test, the battery exhibited 100% capacity retention, an energy efficiency of 61%, and a columbic efficiency of >95% for 100 cycles at 60 mA/cm^2, suggesting the outstanding chemical stability of the $[\mathbf{MV}]\mathbf{Br_2}$ electrolyte.

We then attempted using an anion exchange AMV membrane using Br^- ions as charge carriers to see if it is possible to further improve Coulombic efficiency. A $[\mathbf{MV}]\mathbf{Br_2}$ RFB using the AMV membrane was tested from 20 to 40 mA/cm^2 under the same conditions (Figure S5). However, the $[\mathbf{MV}]\mathbf{Br_2}$ AORFB using the AMV membrane displayed a very poor capacity utilization, only 17.9% at 40 mA/cm^2, and a lower energy efficiency, ca. 55% at 40 mA/cm^2 (see Figure S5ii). It was found that the Br_3^- was trapped by the anion exchange membrane and resulted in a stained yellow membrane, which is believed to increase the membrane resistance (Figure S6). This phenomenon was further confirmed by treating the Br_3^- trapped membrane (yellow color) with $Na_2S_2O_4$ to resume the transparent appearance of the membrane (Figure S6). Consequently, this flow battery was unable to charge/discharge when the current density was greater than 40 mA/cm^2.

For further comparison, we conducted an asymmetric $[\mathbf{MV}]\mathbf{Br_2}$/NaBr AORFB with 0.1 M $[\mathbf{MV}]\mathbf{Br_2}$ as an anolyte and 0.2 M NaBr as a catholyte material with the same porous Daramic membrane as a separator. Despite being slightly more energy-efficient (Figure 3B-ii), this asymmetric flow battery delivered much poorer cycling stability, 65% capacity retention after 100 cycles (Figure 3D, blue curves). It is likely that the formation of the $[\mathbf{MV}](\mathbf{Br_3})_2$ solid phase in the symmetric AORFB leads to the increased electrode resistance and resultant lower energy efficiencies. A postcycling analysis confirmed the crossover of $[MV]^{2+}$ which was present in the catholyte side (Figure S7A). We also conducted another control experiment using *N*-methyl-*N*-ethyl pyrrolidinium bromide (MEP) as a complexing reagent in the asymmetric $[\mathbf{MV}]\mathbf{Br_2}$/NaBr RFB flow battery under the same conditions (Figure 3C). It is found MEP can trap Br_3^- to form a liquid phase when the concentrations of the chemicals are lower than 0.2 M. However, the asymmetric $[MV]Br_2$/(NaBr and MEP) AORFB delivered much worse cycling performance (Figure

https://doi.org/10.1021/acsenergylett.1c01146
ACS Energy Lett. 2021, 6, 2891−2897

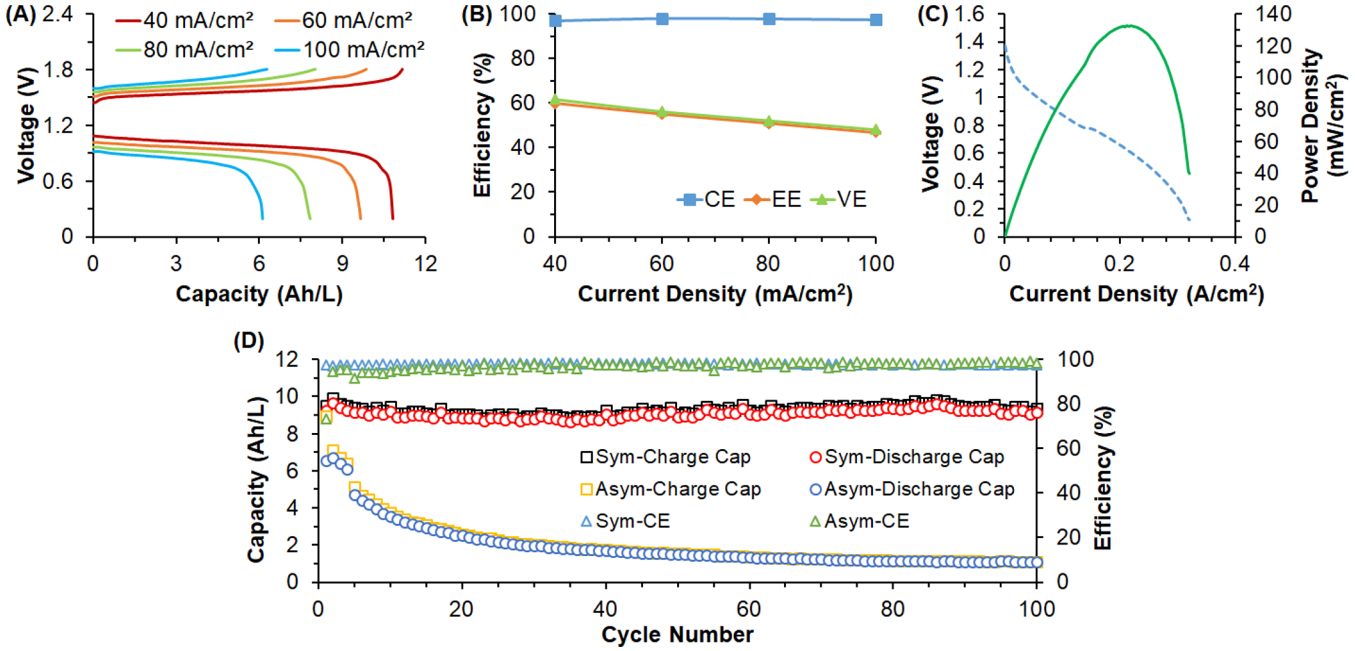

Figure 4. Cycling performance of a symmetric 0.5 [MV]Br_2 AORFB. (A) Representative charge and discharge plots at current densities from 40 to 100 mA/cm². (B) Plots of average Coulombic efficiency (CE), energy efficiency (EE), and voltage efficiency (VE) at different operational current densities. (C) Polarization (dashed curve) and power density (solid curve) data collected at 100% SOC of 0.5 M [MV]Br_2 in 2.0 M NaCl bipolar AORFB with a Daramic membrane. (D) Extended 100 cycle data of the same symmetric [MV]Br_2 AORFB and a control asymmetric MV/Br AORFB.

3D, green curves). After the rate performance studies (Figure 2C-i), the battery capacity dropped to 0.94 Ah/L (ca. 35% capacity utilization). A rapid capacity decay to 0.7 Ah/L was observed within 25 cycles in the extended cycling at 60 mA/cm², and a capacity retention of 74% was recorded after 100 cycles (Figure 2D, green curve). Postcycling studies revealed the crossover of $[MV]^{2+}$ to the opposite electrolyte side (Figure S7B). These control experiments confirm the superior performance of the symmetric **[MV]Br_2** AORFB using the Daramic membrane, which is attributed to the bipolar, self-complexing nature of the **[MV]Br_2** electrolyte.

Finally, the bipolar "self-complexing" **[MV]Br_2** AORFB was demonstrated using 0.5 M **[MV]Br_2** in 2.0 M NaCl supporting electrolyte (164.0 mS/cm) under the same conditions as the 0.1 M flow battery. As shown in Figure 4A,B, the **[MV]Br_2** AORFB was able to operate under 40, 60, 80, and 100 mA/cm² current densities. This battery delivered average columbic efficiencies above 96.5% at each current density, and an energy efficiency was obtained as 60% at an operational current density of 40 mA/cm². The long-term extended cycling performance of the **[MV]Br_2** AORFB was studied at 60 mA/cm² for 100 charge−discharge cycles. As shown in Figure 4D, the 0.5 M **[MV]Br_2** AORFB displayed impressive cycling performance, specifically, after 100 charge−discharge cycles, 100% total capacity retention or 100% capacity retention per cycle with an average energy efficiency of 56% and a Coulombic efficiency of 97.70%. As shown in Figure S8, the charge−discharge curves of the 1st and 100th cycles were nearly overlapped. The polarization curve of the MV/Br AORFB was collected under 100% state of charge (SOC), and a peak power density of 132.7 mW/cm² was recorded as illustrated in Figure 4C. The chemical stability of **[MV]Br_2** during the battery cycling process was confirmed by postcycling analysis using ^{1}H NMR (Figure S9). After the mixing of the catholyte and anolyte after discharge, no new peak could be observed in the ^{1}H NMR spectrum, which indicates that the **[MV]Br_2** electrolyte did not undergo chemical degradation, such as the bromination reaction. We also tested the rate performance of a 1.0 M **[MV]Br_2** AORFB (Figure S10). However, in comparison to the 0.5 M AORFB, the energy, Coulombic, and voltage efficiencies of the 1.0 M AORFB at 60 mA/cm² were clearly reduced to 52.5%, 56.0%, and 93.9%, respectively (Table S1). The results indicate that the lowered energy efficiency was mainly attributed to the reduced Coulombic efficiency, which is most likely associated with the self-discharge through the crossover of the charged, soluble $[MV]^{-\bullet}$ species. The observation highlights that it is necessary to further optimize the porous separator to suppress the crossover.

In stark contrast, an asymmetric MV/Br AORFB using 0.5 M **[MV]Br_2** in 2.0 M NaCl as an anolyte and 1.25 M NaBr in 1.25 M NaCl as a catholyte showed quick capacity fading (>50%) within the first 10 cycles and retained a capacity of only 1.2 Ah/L after 100 cycles, representing ca. 16% capacity retention (Figure 4D). In addition, it is worth noting that the performance metrics of the symmetric, bipolar **[MV]Br_2** AORFB also outperform those of the asymmetric $(SPr)_2V$/NH_4Br and the symmetric (2HO-V)Br_2/MEP/KBr AORFBs, where $(SPr)_2V$ is 1,1′-di(3-sulfonatopropyl)-4,4′-bipyridinium) and (2HO-V)Br_2 is (1,10)-di(2-ethanol)-4,40-bipyridinium dibromide (see a detailed comparison in Table S2).[24,27] For the asymmetric $(SPr)_2V$/NH_4Br AORFB (anolyte, 0.1 M S_2V in 1.0 M NH_4Br; catholyte, 1.2 M NH_4Br and 0.1 M Br_2; 0.67 Wh/L), we had to use excess NH_4Br and Br_2 in the catholyte to compensate the crossover of bromine and achieve 91.% total capacity retention for 100 cycles at 60 mA/cm². The symmetric (2HO-V)Br_2/MEP/KBr AORFB using a mixture of 0.1 M (2HO-V)Br_2, 0.4 M MEP,

https://doi.org/10.1021/acsenergylett.1c01146
ACS Energy Lett. 2021, 6, 2891−2897

and 0.6 M KBr was tested at an energy density of 5.6 Wh/L by using the two-electron storage of (2HO-V)Br_2 and cycled using a capacity control protocol of 78.4%. Although the symmetric (2HO-V)Br_2/MEP/KBr AORFB exhibited 100% capacity for 100 cycles, the cycling stability is questionable because the capacity control would mask any chemical degradation and is thus not recommended for flow battery studies. According to our studies, the use of the negative second electron of viologen molecules (< −0.72 V vs NHE) can lead to unstable cycling because of the chemical discharge by protons to form hydrogen even at pH-neutral conditions ($E(H_2/H^+)$ = −0.41 V vs NHE at pH 7).[9,30] Moreover, in our studies of the asymmetric $MVBr_2$/(NaBr and MEP) AORFB, it was noted that the complexing product, [MEP]Br_3, became a solid phase when the concentrations of MEP and Br_3^- were higher than 0.2 M. Thus, the use of **[MV]Br_2** as a bromine complexing reagent is apparently more advantageous than the use of additional [MEP]Br.

In summary, we designed a novel "self-trapping" MV/Br AORFB using a bipolar electrolyte compound, **[MV]Br_2**, as both anolyte and catholyte at pH-neutral conditions. The formation of the **[MV]$(Br_3)_2$** complex was predicted computationally and confirmed experimentally to be an efficient bromine complexing strategy. In the catholyte side of symmetric MV/Br AORFB, MV could significantly avoid the bromine species crossover which results in stable cycling performance in comparison to the asymmetric MV/Br AORFB. The demonstrated symmetric MV/Br AORFB delivered 100% capacity retention in 100 charge−discharge cycles and a power density of 133 mW/cm^2. The performance metrics and low cost of the pH-neutral bipolar **[MV]Br_2** AORFBs make it a promising solution to large-scale energy storage. The newly discovered self-complexing strategy of **[MV]Br_2** reported herein will inspire the development of low-cost, high-performance AORFBs using new bipolar viologen bromide molecules and other molecular designs.

■ ASSOCIATED CONTENT

Supporting Information

The Supporting Information is available free of charge at https://pubs.acs.org/doi/10.1021/acsenergylett.1c01146.

Experimental details and NMR, UV−vis, Raman, electrochemical, and computational data (PDF)

■ AUTHOR INFORMATION

Corresponding Author

T. Leo Liu − *Department of Chemistry and Biochemistry, Utah State University, Logan, Utah 84322, United States;* orcid.org/0000-0002-3698-1096; Email: leo.liu@usu.edu, liugrouppub@gmail.com

Authors

Wenda Wu − *Department of Chemistry and Biochemistry, Utah State University, Logan, Utah 84322, United States*

Jian Luo − *Department of Chemistry and Biochemistry, Utah State University, Logan, Utah 84322, United States*

Fang Wang − *Department of Chemistry and Biochemistry, Utah State University, Logan, Utah 84322, United States*

Bing Yuan − *State Key Laboratory Base of Eco-chemical Engineering, College of Chemistry and Molecular Engineering, Qingdao University of Science and Technology, Qingdao 266042, China;* orcid.org/0000-0003-1904-8146

Complete contact information is available at: https://pubs.acs.org/10.1021/acsenergylett.1c01146

Notes

The authors declare the following competing financial interest(s): A patent application containing the results in the submitted manuscript was filed.

■ ACKNOWLEDGMENTS

We thank the National Science Foundation (Career Award, Grant No. 1847674) and Utah State University (faculty startup funds to Dr. T. Leo Liu) for supporting this study. Dr. Bin Yuan is grateful for China CSC Abroad Studying Fellowship to support her study at USU. We acknowledge that the NMR studies are supported by NSF's MRI program (Award Number 1429195).

■ REFERENCES

(1) Luo, J.; Hu, B.; Hu, M.; Zhao, Y.; Liu, T. L. Status and Prospects of Organic Redox Flow Batteries towards Sustainable Energy Storage. *ACS Energy Lett.* **2019**, *4*, 2220−2236.

(2) Hu, B.; Luo, J.; Debruler, C.; Hu, M.; Wu, W.; Liu, T. L. In "Redox-Active Inorganic Materials for Redox Flow Batteries. *Ency. Inorg. Bioinorg. Chem.* **2019**, 1−25.

(3) Winsberg, J.; Hagemann, T.; Janoschka, T.; Hager, M. D.; Schubert, U. S. Redox-Flow Batteries: From Metals to Organic Redox-Active Materials. *Angew. Chem., Int. Ed.* **2017**, *56*, 686−711.

(4) Ding, Y.; Zhang, C.; Zhang, L.; Zhou, Y.; Yu, G. Molecular engineering of organic electroactive materials for redox flow batteries. *Chem. Soc. Rev.* **2018**, *47*, 69−103.

(5) Wang, W.; Luo, Q.; Li, B.; Wei, X.; Li, L.; Yang, Z. Recent Progress in Redox Flow Battery Research and Development. *Adv. Funct. Mater.* **2013**, *23* (8), 970−986.

(6) Janoschka, T.; Martin, N.; Martin, U.; Friebe, C.; Morgenstern, S.; Hiller, H.; Hager, M. D.; Schubert, U. S. An Aqueous, Polymer-based Redox-Flow Battery Using Non-corrosive, Safe, and Low-cost Materials. *Nature* **2015**, *527* (7576), 78−81.

(7) Liu, T.; Li, B.; Wei, X.; Nie, Z.; Sprenkle, V.; Wang, W. Aqueous Electrolytes for Redox Flow Batteries. US20160308233A1, 2015.

(8) Janoschka, T.; Martin, N.; Hager, M. D.; Schubert, U. S. An Aqueous Redox-Flow Battery with High Capacity and Power: The TEMPTMA/MV System. *Angew. Chem., Int. Ed.* **2016**, *55* (46), 14427−14430.

(9) DeBruler, C.; Hu, B.; Moss, J.; Liu, X.; Luo, J.; Sun, Y.; Liu, T. L. Designer Two-Electron Storage Viologen Anolyte Materials for Neutral Aqueous Organic Redox Flow Batteries. *Chem.* **2017**, *3*, 961.

(10) Hu, B.; DeBruler, C.; Rhodes, Z.; Liu, T. L. Long-Cycling Aqueous Organic Redox Flow Battery (AORFB) toward Sustainable and Safe Energy Storage. *J. Am. Chem. Soc.* **2017**, *139* (3), 1207−1214.

(11) Hu, B.; Luo, J.; Hu, M.; Yuan, B.; Liu, T. L. A pH Neutral, Metal Free Aqueous Organic Redox Flow Battery Employing an Ammonium Anthraquinone Anolyte. *Angew. Chem., Int. Ed.* **2019**, *58*, 16629−16636.

(12) Luo, J.; Hu, B.; Debruler, C.; Bi, Y.; Zhao, Y.; Yuan, B.; Hu, M.; Wu, W.; Liu, T. L. Unprecedented Capacity and Stability of Ammonium Ferrocyanide Catholyte in pH Neutral Aqueous Redox Flow Batteries. *Joule* **2019**, *3*, 149.

(13) Hoober-Burkhardt, L.; Krishnamoorthy, S.; Yang, B.; Murali, A.; Nirmalchandar, A.; Prakash, G. K. S.; Narayanan, S. R. A New Michael-Reaction-Resistant Benzoquinone for Aqueous Organic Redox Flow Batteries. *J. Electrochem. Soc.* **2017**, *164* (4), A600−A607.

(14) Hollas, A.; Wei, X.; Murugesan, V.; Nie, Z.; Li, B.; Reed, D.; Liu, J.; Sprenkle, V.; Wang, W. A Biomimetic High-capacity Phenazine-based Anolyte for Aqueous Organic Redox Flow Batteries. *Nat. Energy* **2018**, *3* (6), 508−514.

(15) Chen, Y.; Zhou, M.; Xia, Y.; Wang, X.; Liu, Y.; Yao, Y.; Zhang, H.; Li, Y.; Lu, S.; Qin, W.; Wu, X.; Wang, Q. A Stable and High-Capacity Redox Targeting-Based Electrolyte for Aqueous Flow Batteries. *Joule* **2019**, *3* (9), 2255−2267.
(16) Zhang, C.; Niu, Z.; Peng, S.; Ding, Y.; Zhang, L.; Guo, X.; Zhao, Y.; Yu, G. Phenothiazine-Based Organic Catholyte for High-Capacity and Long-Life Aqueous Redox Flow Batteries. *Adv. Mater.* **2019**, *31* (24), 1901052.
(17) Ji, Y.; Goulet, M.-A.; Pollack, D. A.; Kwabi, D. G.; Jin, S.; Porcellinis, D.; Kerr, E. F.; Gordon, R. G.; Aziz, M. J. A Phosphonate-Functionalized Quinone Redox Flow Battery at Near-Neutral pH with Record Capacity Retention Rate. *Adv. Energy Mater.* **2019**, *9* (12), 1900039.
(18) Medabalmi, V.; Sundararajan, M.; Singh, V.; Baik, M.-H.; Byon, H. R. Naphthalene diimide as a two-electron anolyte for aqueous and neutral pH redox flow batteries. *J. Mater. Chem. A* **2020**, *8* (22), 11218−11223.
(19) Hu, B.; Liu, T. L. Two Electron Utilization of Methyl Viologen Anolyte in Nonaqueous Organic Redox Flow Battery. *J. Energy Chem.* **2018**, *27*, 1326−1332.
(20) Luo, J.; Hu, B.; Sam, A.; Liu, T. L. Metal-Free Electrocatalytic Aerobic Hydroxylation of Arylboronic Acids. *Org. Lett.* **2018**, *20* (2), 361−364.
(21) Luo, J.; Liu, T. L. Tandem Solar Flow Batteries for Conversion, Storage, and Utilization of Solar Energy. *Chem.* **2018**, *4* (11), 2488−2490.
(22) Beh, E. S.; De Porcellinis, D.; Gracia, R. L.; Xia, K. T.; Gordon, R. G.; Aziz, M. J. A Neutral pH Aqueous Organic−Organometallic Redox Flow Battery with Extremely High Capacity Retention. *ACS Energy Lett.* **2017**, *2*, 639−644.
(23) DeBruler, C.; Hu, B.; Moss, J.; Luo, J.; Liu, T. L. A Sulfonate-Functionalized Viologen Enabling Neutral Cation Exchange, Aqueous Organic Redox Flow Batteries toward Renewable Energy Storage. *ACS Energy Lett.* **2018**, *3*, 663−668.
(24) Luo, J.; Wu, W.; Debruler, C.; Hu, B.; Hu, M.; Liu, T. L. A 1.51 V pH neutral redox flow battery towards scalable energy storage. *J. Mater. Chem. A* **2019**, *7* (15), 9130−9136.
(25) Rumble, J. *CRC Handbook of Chemistry and Physics*, 100th ed.; CRC Press, 2019.
(26) *Mineral Commodity Summaries*. https://www.usgs.gov/centers/nmic/mineral-commodity-summaries. U.S. Geological Survey, 2020.
(27) Liu, W.; Liu, Y.; Zhang, H.; Xie, C.; Shi, L.; Zhou, Y.-G.; Li, X. A highly stable neutral viologen/bromine aqueous flow battery with high energy and power density. *Chem. Commun.* **2019**, *55* (33), 4801−4804.
(28) Mastragostino, M.; Valcher, S. Polymeric salt as bromine complexing agent in a Zn-Br2 model battery. *Electrochim. Acta* **1983**, *28* (4), 501−505.
(29) Bauer, G.; Drobits, J.; Fabjan, C.; Mikosch, H.; Schuster, P. Raman spectroscopic study of the bromine storing complex phase in a zinc-flow battery. *J. Electroanal. Chem.* **1997**, *427* (1), 123−128.
(30) Hu, B.; Tang, Y.; Luo, J.; Grove, G.; Guo, Y.; Liu, T. L. Improved Radical Stability of Viologen Anolytes in Aqueous Organic Redox Flow Batteries. *Chem. Commun.* **2018**, *54*, 6871−6874.

https://doi.org/10.1021/acsenergylett.1c01146
ACS Energy Lett. 2021, 6, 2891−2897